

# Design, Realization and Sensorization of the Dexterous iCub Hand

Alexander Schmitz, Ugo Pattacini, Francesco Nori, Lorenzo Natale, Giorgio Metta and Giulio Sandini

**Abstract**—In this paper we describe the hand of the humanoid iCub, an open source robotic platform funded by the European Commission. The principal design rationale was the necessity to supply the robot with sufficiently dexterous and sensorized hands in order to study complex skills such as manipulation. The final design has 9 actuators for each hand, 12 tactile sensors at each fingertip, 48 pressure sensors in the palm and 17 position sensors. The electronics for the sensors are embedded in the hand. As a preliminary application we tested the hand in a simplified grasping scenario in order to quantitatively evaluate the reliability and repeatability of the overall system.

## I. INTRODUCTION

During the last thirty years, robotic research has received an increasing interest driven by the goal of realizing machines capable of robustly manipulating objects in the environment. In this context the design of sophisticated and sensorized robotic hands has fundamental importance. Moreover, development in this field has been recently boosted by innovative research trends based on the idea that perception is an active process, where agents actively structure their own sensory input by manipulating the world to obtain “good” sensory data, thus enhancing categorization, adaptation and learning (see for example [1], [2], [3]).

In this paper we describe the hand of the iCub, an open-source humanoid robot developed to study manipulation. The paper is organized as follows: Section I-A gives an overview of previous approaches to the design of robotic hands; Section II briefly describes the iCub platform; Section III presents the iCub hand focusing in particular on the actuation system (Section III-A), the proprioceptive sensors (Section III-B) and the sensorized fingertips and palm (Section III-C); Section IV describes a simple scenario that we have implemented to evaluate the reliability of the overall structure; finally Section V presents the conclusion and future works.

### A. Previous hands design choices

The beginning of robotic hands design dates back to the early seventies and a complete tutorial on previous design

Alexander Schmitz is with the Italian Institute of Technology, 16163 Genova, Italy and the Department of Automatic Control and Systems Engineering, University of Sheffield, Sheffield, UK S1 3JD. alexander.schmitz@iit.it

Ugo Pattacini, Francesco Nori, Lorenzo Natale and Giulio Sandini are with the Italian Institute of Technology, 16163 Genova, Italy. ugo.pattacini@iit.it, francesco.nori@iit.it, lorenzo.natale@iit.it, giulio.sandini@iit.it

Giorgio Metta is with the Italian Institute of Technology, 16163 Genova, Italy and the Dipartimento di Informatica Sistemistica e Telematica, Università degli Studi di Genova, 16145 Genoa, Italy. giorgio.metta@iit.it

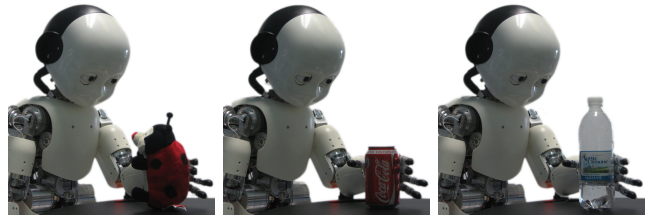


Fig. 1. The iCub while grasping three different objects.

choices is outside the scope of this paper. We will focus therefore on a subset of previous approaches starting from one of the first designs, the Utah/MIT hand [4], which was the ancestor of a long series of tendon based solutions. Since tendons allows the realization of compact and light-weight solutions, they have been typically employed to realize robotic hands that could be easily integrated (an example is the Robonaut-2 platform [5]). An exception is the work of [6], in which a carefully designed light weight arm supports the heavy payload of a hand that does not use tendons. Other designs such as the Shadow hand [7] have optimized the dexterity and sensorization (20 degrees of freedom, tendon tension measurements and quantum tunneling composites based tactile fingertips). Similarly, other projects have focused on sensorization: the Obrero hand [8] for example has 40 highly sensitive contact points embedding 4 Hall effect sensors each. Some other designs, such as the UB-hand [9], have explored the possibility of reducing costs while increasing compliance without compromising the hand dexterity.

## II. THE ICUB PLATFORM

The iCub humanoid robot has been designed with the goal of creating an open hardware/software robotic platform for research in embodied cognition [10]. Its design has been mainly developed within the RobotCub project<sup>1</sup>, a European funded project with the aim of studying natural and artificial cognitive systems [11]. At the current state, the iCub robot has a total of 53 actuated degrees of freedom, 6 in each leg, 7 in each arm, 6 in the head, 3 in the waist and 9 for each hand.

## III. THE ICUB HAND

In this section we describe the overall structure and sensors of the iCub hand. Differently from other projects, the hand has been specifically designed for the iCub and therefore

<sup>1</sup>RobotCub was a project funded by the European Commission under the sixth framework programme (FP6) by Unit E5: Cognitive system, interaction and Robotics.

an exceptional level of integration was achieved allowing high dexterity and sensorization in limited dimensions. Early versions of the hand were presented in [12] and [13].

### A. The hand actuation system

The hand actuation system is based on tendons. This solution was adopted because it allowed maintaining a sufficient dexterity in the available space. Most of the motors are integrated in the forearm and the associated tendons are routed through the wrist. Only two motors are embedded in the palm. The adopted tendon actuation can be divided into two different classes: *open-ended* tendon drives and *closed-loop* tendon drives (see [14] for details).

The typical closed-loop actuation structure relies on a pulley attached to the motor: a stainless steel tendon<sup>2</sup> is twined around the pulley and is *routed to the joint and back to the motor* using custom made guide-wires. These guide-wires basically consists of long Teflon-coated springs (1mm in diameter) inside which the tendons slide. Therefore, the closed-loop configuration uses the tendon for moving the joint in both directions of motion. On the contrary, in the open-ended actuation system the tendon is only used to rotate the joint in one direction (usually flexion) while a spring is in charge of rotating the joint back (extension). The rotation of the motor flexes the joint and compresses the spring; the counter-rotation releases the potential energy accumulated in the spring and extends the joint.

The hand has 19 joints. Its dimensions (155mm long, 75mm wide at the fingers and 40mm thick) and ranges of motion (90° for all joints except for the abduction of the fingers, which is for all fingers together around 50°) were inspired by those of a human hand. Most of the human hand joints have been replicated. The thumb has four joints: two of them are located in the carpometacarpal (CMC) joint while the other two joints are in the metacarpophalangeal (MP) joint and in the interphalangeal (IP) joint respectively. Similarly the remaining four fingers (index, middle, ring and little) have four joints each: two located in the metacarpophalangeal (MP) joint and the other two in the proximal interphalangeal (PIP) joint and in the distal interphalangeal (DIP) joint respectively (see Fig. 2 for a detailed description).

The actuation of all these 19 joints is obtained using 9 DC motors, 7 of which are embedded in the forearm and 2 in the hand. Therefore, certain degrees of motion (DOM) are obtained by coupling different joints so that they are moved by a single motor in a synergistic fashion (see Fig. 3 and 4). Only the abduction of the fingers is coupled tightly, the others elastically, resulting in some passive degrees of freedom. Even though this is a major difference between the iCub hand mechanics and the human hand biomechanics, the idea of reducing the overall number of motors by creating suitable synergies was suggested by well established studies on typical grasping strategies [17]. In the following, we give a detailed description of the joints couplings; nominally we

<sup>2</sup>We used commercial steel cables produced by Carlstahl [15] with  $\varnothing = 0.63mm$ . Also other materials such as Dyneema [16] were tested but were eventually not chosen because of their tendency to wear on the motor pulley.

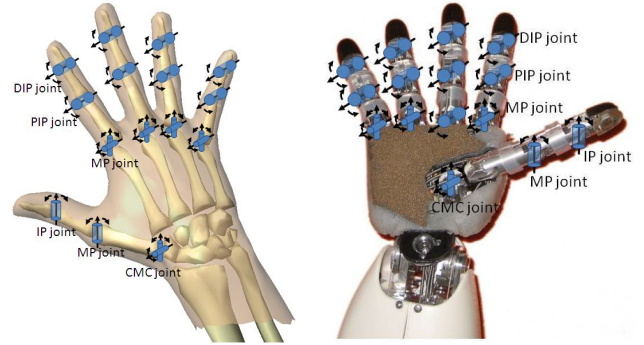


Fig. 2. **Left:** a sketch of the human hand with its joints; joints name for the middle, ring and little fingers are the same indicated for the index finger. **Right:** a picture of the iCub hand with all its joints; notice the analogy with the human hand joints.

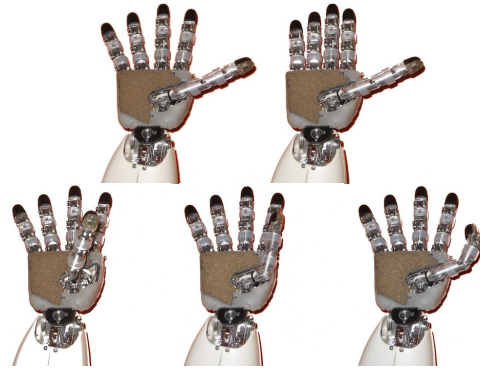


Fig. 3. 4 DOMs of the iCub hand. From the top-left corner (reading order): (1) initial configuration for all successive postures; (2) (index, middle, ring, little) fingers MP abduction, (3) thumb MP opposition, (4) thumb MP abduction, (5) thumb MP-IP coupling.

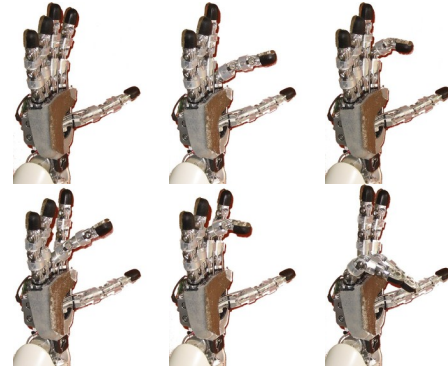


Fig. 4. 5 DOMs of the iCub hand. From the top-left corner (reading order): (1) initial configuration for all successive postures; (2) index MP flexion, (3) index PIP-DIP coupling, (4) middle MP flexion, (5) middle PIP-DIP coupling, (6) ring-little fingers coupling.

describe the finger MP abduction coupling, the thumb MP-IP coupling, the index PIP-DIP coupling, the middle PIP-DIP coupling and finally the ring-little fingers coupling.

1) *Fingers MP abduction coupling:* a single motor embedded in the hand is used to actuate the index (abbreviated *ind*), ring (*rng*) and little (*ltl*) fingers abduction/adduction movements. The mechanism is basically a closed-loop tendon drive with the tendon twined around the index, ring and

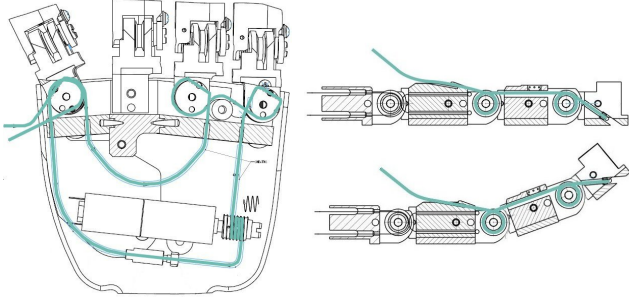


Fig. 5. **Left:** a cross section of the fingers MP abduction/adduction actuation scheme. The configuration is a closed-loop tendon drive; the tendon path is highlighted in cyan. The joint pulley radii and the tendon winding direction (clock-wise or counter clock-wise) determine the value and the sign of the coefficients in Eq. (1). **Right:** a cross section of the distal joints actuation scheme (thumb MP-IP, index and middle PIP-DIP coupling). The configuration is an open-ended drive; tendon path is highlighted in cyan. The top figure shows the straight finger while the bottom refers to the flexed finger. The coordination of the two joints movement by means of a single motor is obtained by torsional springs; steady state configuration in absence of external forces is give by Eq. (2). The picture shows the flexion steady state configuration when  $k_{ip} = k_{mp}$ .

little finger pulleys in order to coordinate their movements (see Fig. 5). Given a rotation  $\theta_m$  of the motor, the MP abduction/adduction displacement for each finger is given by the following formulas:

$$\theta_{ind} = \frac{r_m}{r_{ind}} \theta_m, \quad \theta_{rng} = -\frac{r_m}{r_{rng}} \theta_m, \quad \theta_{ttl} = -\frac{r_m}{r_{ttl}} \theta_m \quad (1)$$

where  $\theta_{finger}$  is the finger MP abduction/adduction displacement,  $r_m = 3.25mm$  is the radius of the motor pulley,  $r_{finger}$  is the radius of the finger pulley ( $r_{ind} = 4.75mm$ ,  $r_{rng} = 4.75mm$ ,  $r_{ttl} = 3.5mm$ ). Therefore, the radii of the joint pulleys determine the finger coordination.

2) *Thumb MP-IP coupling:* the thumb distal joints are actuated by an open-ended tendon drive. The coupling of the joints is obtained by winding the cable around both the MP and the IP joints (see Fig. 5 right). A torsional spring in both the MP and IP joints accumulates energy when the motor is pulling the cable, thereby flexing the joints. This potential energy is then used for extending the finger. At the equilibrium configuration and *in absence of external forces*, the position of the MP-IP joints ( $\theta_{mp}$ ,  $\theta_{ip}$ ) is related to the position of the motor ( $\theta_m$ ) by the following rules:

$$\theta_{mp} = \frac{k_{ip}}{k_{mp} + k_{ip}} \frac{r_m}{r_{mp}} \theta_m, \quad \theta_{ip} = \frac{k_{mp}}{k_{mp} + k_{ip}} \frac{r_m}{r_{ip}} \theta_m \quad (2)$$

where  $k_{ip}$  and  $k_{mp}$  are the stiffnesses of the torsional springs attached to the IP and MP joints,  $r_m$  is the radius of the motor pulley and  $r_{ip} = r_{mp}$  are the radii of the IP and MP joint pulleys.

3) *Index and middle PIP-DIP couplings:* the index finger distal joints (PIP and DIP) are actuated by a single motor according to the same actuation structure described for the thumb MP and IP joints. The same actuation structure has also been adopted for the distal joints of the middle finger.

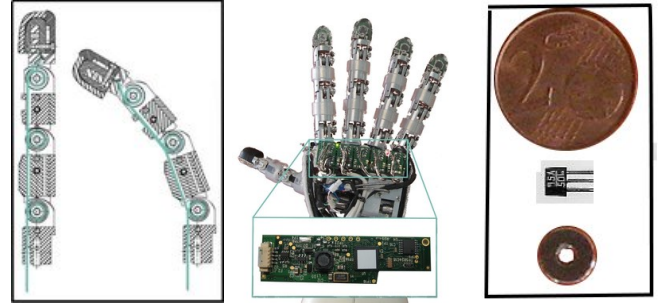


Fig. 6. **Left:** cross section of the ring finger actuation scheme (little finger has an identical actuation scheme). The design is an open-ended tendon drive similar to the one used for the thumb, index and middle fingers distal joints (Fig. 5 right) but in this case three joints are coupled together instead of two. **Center:** a picture of the hand with a zoom on the embedded board designed to collect the analog data from the 17 (Hall effect) position sensors. **Right:** a picture of the analog Hall effect sensor together with the ring-shaped magnet used to generate the magnetic field sensed by the sensor. Magnets are positioned at each joint with the sensor underneath the magnet.

4) *Ring and little finger joint coupling:* the little and ring finger joints (MP flexion/extension, DIP and PIP joints) are moved by a single motor with a suitable coupling mechanism. In the current configuration, a closed-loop tendon moves a linear slider; the slider is then used to pull simultaneously two open-ended tendon drives: one tendon moves the little finger; the other tendon actuates the ring finger. Specifically, each tendon actuates the MP (flexion/extension), DIP and PIP joints according to a three joints extension of the coupling mechanism used in the thumb, index and middle finger distal joints (see Fig. 6 left). In this case (at steady state and in absence of external forces) the motor position  $\theta_m$  and the joint positions  $\theta_{mp}$ ,  $\theta_{dip}$  and  $\theta_{pip}$  satisfy the following equations (holding for both ring and little fingers):

$$\theta_{mp} = \frac{1}{k_{mp}} \frac{1}{\frac{1}{k_{mp}} + \frac{1}{k_{pip}} + \frac{1}{k_{dip}}} \frac{r_m}{r_{mp}} \theta_m, \quad (3)$$

$$\theta_{pip} = \frac{1}{k_{pip}} \frac{1}{\frac{1}{k_{mp}} + \frac{1}{k_{pip}} + \frac{1}{k_{dip}}} \frac{r_m}{r_{pip}} \theta_m, \quad (4)$$

$$\theta_{dip} = \frac{1}{k_{dip}} \frac{1}{\frac{1}{k_{mp}} + \frac{1}{k_{pip}} + \frac{1}{k_{dip}}} \frac{r_m}{r_{dip}} \theta_m, \quad (5)$$

where  $k_{mp}$ ,  $k_{pip}$  and  $k_{dip}$  are the stiffnesses of the torsional springs attached to the MP, PIP and DIP joints,  $r_m$  is the radius of the motor pulley,  $r_{mp} = r_{pip} = r_{dip}$  are the radii of the MP, PIP and DIP joint pulleys.

5) *Uncoupled joints:* 4 out of 19 joints are driven by a single motor without any coupling. These joints are the thumb CMC opposition, the thumb CMC abduction/adduction, the index MP flexion/extension and the middle MP flexion/extension. For these joints the actuation structure consists of a closed-loop tendon drive and therefore the position of the motor  $\theta_m$  is related to the position of the joint  $\theta_j$  by the following formula:

$$\theta_m = \frac{r_m}{r_j} \theta_j, \quad (6)$$

where  $r_m$  and  $r_j$  are the radius of the motor pulley and of the joint pulley respectively.

6) *Summary*: the overall hand actuation structure is summarized in Table I. The 19 joints are reported on the horizontal axis where thumb  $CMC_1$  is the thumb opposition, thumb  $CMC_2$  is the thumb abduction/adduction,  $MP_1$  is the abduction/adduction,  $MP_2$  is the flexion/extension. The 9 DOMs are reported in the vertical axis. If a DOM contributes to moving a certain joint then the corresponding entry in the table differs from “-” and it contains a reference to the equation that describes the relationship between the motor and joint position.

### B. The phalangeal position sensors

The positions of 17 out of 19 hand joints (indicated with  $\checkmark$  in Table I) are measured with tiny Hall effect sensors (SS495A Honeywell, Fig. 6 right) whose analog output is converted to digital by a custom made board (see Fig. 6 center). This board has been produced in two different (symmetric) form factors in order to be optimally embedded in the right and left hand. The 12 bits analog to digital conversion of the 17 signals relies on a 16 bit DSP Microchip (dsPIC30F4013) and on a multiplexer (ADG659). The digital data is transmitted to the control board via a CAN-bus.

1) *Grasp detector*: Open-ended tendon drives such as the ones used in the iCub hand distal joints can be used to detect the presence of external forces. In practice, the coupling equations, “(2)” or “(3), (4) and (5)”, hold only in absence of external forces. Therefore, exploiting the joints position measurement  $(\theta_{mp}, \theta_{ip}, \theta_{pip}, \theta_{dip})$  for the different fingers, it is possible to determine the presence of external forces by checking the validity of the coupling equations. Remarkably, the coupling equations can always be written as a one dimensional linear space embedded in an  $n$ -dimensional space:

$$\mathbf{q} \in \mathbb{R}^n \text{ s.t. } \mathbf{q} = \mathbf{q}_1 \cdot t + \mathbf{q}_0, \quad t \in [t_{min}, t_{max}]. \quad (7)$$

In the case of (2),  $n = 2$ :

$$\mathbf{q} = \begin{bmatrix} \theta_{mp} \\ \theta_{ip} \end{bmatrix}, \quad \mathbf{q}_1 = \begin{bmatrix} \frac{k_{ip}}{k_{mp}+k_{ip}} r_m \\ \frac{k_{mp}}{k_{mp}+k_{ip}} r_m \end{bmatrix}, \quad t = \theta_m, \quad (8)$$

$[t_{min}, t_{max}]$  corresponds to the range of the motor rotation.  $\mathbf{q}_0$  accounts for the springs rest-length and possible offsets in the motor position and/or in the joint measurements. Fitting (7) to a dataset of joint positions (collected in absence of external forces) requires simple linear algebra tools (see [18] for details). Once the model has been built, the distance of an arbitrary configuration  $\mathbf{q}$  from the model (7) can reveal the presence of an external force on the finger. This distance gives also a qualitative idea of the intensity of the external force: the greater the distance from the model the higher the force. Exploiting this idea a grasp detector has been created; the associated software is available (together with other tools, modules, applications and further documentation) in the iCub open source repository [18].

### C. Skin sensors

We have equipped the hands of iCub with a distributed pressure sensing system based on capacitive technology. In

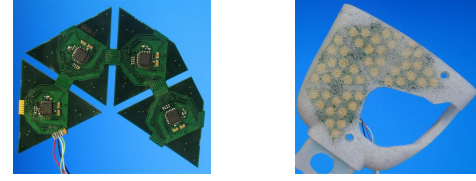


Fig. 7. **Left**: a picture of triangular PCBs before being embedded in the palm. Each triangular module includes an AD7147 chip visible in the middle of the triangles. **Right**: a picture of the sensorized palm without the Lycra conductive layer. The visible white foam acts as a deformable dielectric for the capacitive pressure sensor and guarantees the compliance of the sensor. Also visible are the round pads on the triangular modules. The sensor delivers one capacitance measurements for each round pad.

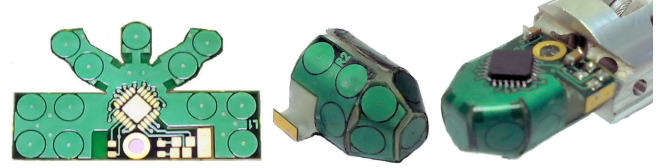


Fig. 8. **Left**: a picture of flexible PCB before being wrapped around the fingertip. The 12 round pads for the capacitive pressure sensor system are visible as well as the soldering points for the AD7147 chip. **Center**: a picture of the flexible PCB wrapped around the inner support. The inner support is printed with a 3D printer (Eden 3D printer from *Objet*). **Right**: a picture of the fingertip without the fingernail and the soft silicone foam.

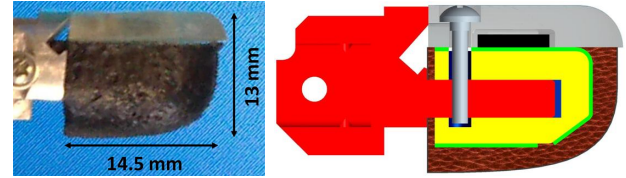


Fig. 9. **Left**: a close-up picture of the fingertip. **Right**: cross-section of the fingertip. The inner support of the fingertip is shown in yellow, and the flexible PCB that is wrapped around it is depicted in green. To mechanically attach the fingertip to the hand, the last phalanx of each digit (shown in red) has a stick that fits inside a hole in the inner support. A screw is used to secure the fingertip and in addition the screw fixes a fingernail on top of the fingertip that covers the PCB. The dielectric made of silicone rubber foam is depicted in brown, and around the foam there is the carbon black layer. The AD7147 chip is also shown in black.

particular, the skin of the palm incorporates four triangular modules which provide 12 pressure measurements each, and also each of the five fingertips provides 12 pressure measurements (giving the sum of 108 sensitive elements per hand). To obtain the 12 measurements, each triangular palm module and each fingertip incorporates a flexible printed circuit board (PCB), which has 12 round pads, one for each sensitive element, which are connected to a capacitive to digital converter chip (AD7147 from *Analog Devices*), which can collect and send 12 measurements of capacitance over an I<sup>2</sup>C serial bus. The flexible PCBs of the palm can be used to cover generic curved surfaces (see Fig. 7), while the small size and very curved shape of the fingertips made it necessary to design a specialized PCB which can be wrapped around the inner support of the fingertip (see Fig. 8). Because the PCBs provide a serial interface, the fingertip connections require only 4 wires each, which are routed along the sides

TABLE I

A TABULAR REPRESENTATION OF THE SYNERGIES USED TO MOVE THE 19 JOINTS BY MEANS OF 9 MOTORS (SEE SECTION III-A.6).

DOM	Joints																		
	thumb				index				middle			ring				little			
	CMC <sub>1</sub>	CMC <sub>2</sub>	MP	IP	MP <sub>1</sub>	MP <sub>2</sub>	PIP	DIP	MP <sub>2</sub>	PIP	DIP	MP <sub>1</sub>	MP <sub>2</sub>	PIP	DIP	MP <sub>1</sub>	MP <sub>2</sub>	PIP	DIP
Finger MP abduction	-	-	-	-	(1)	-	-	-	-	-	-	(1)	-	-	-	(1)	-	-	-
Thumb MP opposition	(6)	-	-	-	-	-	-	-	-	-	-	-	-	-	-	-	-	-	-
Thumb MP abduction	-	(6)	-	-	-	-	-	-	-	-	-	-	-	-	-	-	-	-	-
Thumb MP-IP coupling	-	-	(2)	(2)	-	-	-	-	-	-	-	-	-	-	-	-	-	-	-
Index MP flexion	-	-	-	-	-	(6)	-	-	-	-	-	-	-	-	-	-	-	-	-
Index PIP-DIP coupling	-	-	-	-	-	-	(2)	(2)	-	-	-	-	-	-	-	-	-	-	-
Middle MP flexion	-	-	-	-	-	-	-	-	(6)	-	-	-	-	-	-	-	-	-	-
Middle PIP-DIP coupling	-	-	-	-	-	-	-	-	-	(2)	(2)	-	-	-	-	-	-	-	-
Ring-little coupling	-	-	-	-	-	-	-	-	-	-	-	-	(3)	(4)	(5)	-	(3)	(4)	(5)
Position Measurement	✓	✓	✓	✓	✓	✓	✓	✓	✓	✓	✓	✓	✓	✓	✓	✓	✓	✓	✓

of the fingers. The PCBs in the palm are also electrically connected to each other and only one of them needs to be connected with wires. All the data is collected by a small micro-controller board, which is located in the forearm of the robot and sends the measurements via a CAN-bus.

Above the flexible PCBs in the palm and the fingertips is a roughly 2mm thick layer of soft silicone foam (Soma Foama 15 from *Smooth-On*). It acts as a dielectric for the capacitive pressure sensor and makes the sensor compliant. On top of the foam there is a second conductive layer: electrically conductive Lycra for the palms, electrically conductive silicone for the fingertips (see Fig. 9). This layer is connected to ground and enables the sensor to respond to objects irrespective of their electrical properties (for details please refer to [19]). In addition, this layer reduces electronic noise from the environment. When pressure is applied to the sensor, this conductive layer gets closer to the round pads on the PCB and thereby changes their capacitance. We use this change in capacitance as an estimation of the pressure applied to the sensor.

#### IV. EXPERIMENT

In this section we describe an experiment that was conducted to test the reliability and repeatability of sensory data during a sequence of grasp movements: A set of objects was positioned in the same location on a table in front of the iCub. The robot performed a preprogrammed movement to reach for the objects in Fig. 1: a plush ladybug, a coke can and a plastic bottle. Once the movement was completed, the iCub performed a grasping action. The latter was implemented as a predefined (position controlled) closure of the fingers. In this experiment, the hypothesis is that the same haptic stimulus can be produced on the sensors during different trials. This happens if: (1) the object is in the same position/configuration with respect to the hand and (2) the fingers execute the same movement. The first hypothesis can be approximated by adopting sufficient care in positioning the object; the second was verified *a-posteriori* by measuring the variability on the position measurements of the joints of the hand: Table II reports the movement variability when 4 different grasping actions were repeated 20 times. Results show that movements were relatively repeatable, as confirmed by the small standard deviation of the recorded data (for example the little finger DIP joint was measured

to have a maximum standard deviation of  $4.24deg$ , when grasping the can).

Given the assumption of repeatable haptic stimuli, we tested the reliability of the tactile sensors in 20 repeated grasping trials. Fig. 10 shows the results: red lines refer to the average sensor response when performing the grasping movement with no object; black lines and shaded regions represent respectively the average and standard deviation of the response while performing the grasping. Different rows refer to different fingers (from the top thumb, index, middle, ring and little); columns 1, 3 and 5 refer to the fingertip sensor responses and columns 2, 4 and 6 to the grasp detector described in Section III-B.1. Among the 12 sensitive elements in each fingertip we plotted the one with the strongest response (measured as the difference between the response corresponding to the condition in which the hand grasp each object or is left empty). The plots corresponding to the grasp detector show the output of the module, i.e. at time  $t$  the distance between the current hand configuration and the configuration predicted by the model calibrated as explained in Section III-B.1.

Results clearly show the reliability of the fingertip sensors and demonstrate that their response can be used to detect the contact with the objects. The time of contact is indicated in the horizontal axis (time ticks in the horizontal axis are at 0, 5 and 10 seconds. If a contact is detected, an additional tick is added). It was inferred by monitoring the difference between the current response and the 95% confidence interval on the response without object (red line). On the other side, the grasp detector module sometimes fails to detect contact (e.g. detection failed on the ring finger in the coke and the ladybug objects and on the middle and ring fingers during grasping of the coke and bottle). However it is fair to say that in the experiments reported in this paper the model of eq. (8) was tuned using data from generic hand postures. The performance can be improved if the grasp detector is trained on the data obtained from the more specific movements performed in these experiments.

#### V. CONCLUSION AND FUTURE WORKS

In this paper we described the hand of the iCub. The hand is the result of a design that optimized the level of integration of the hand in the overall robot to meet the project specifications in terms of dimensions, dexterity and sensorization. For example the hand DOMs are actuated

TABLE II

A TABULAR DESCRIPTION OF THE MOVEMENT VARIABILITY IN DIFFERENT GRASPING ACTIONS.

Grasped object	Joints movements variability during different grasping actions: standard deviation in degrees																			
	thumb				index				middle				ring				little			
	CMC <sub>1</sub>	CMC <sub>2</sub>	MP	IP	MP <sub>2</sub>	PIP	DIP	MP <sub>1</sub>	MP <sub>2</sub>	PIP	DIP	MP <sub>1</sub>	MP <sub>2</sub>	PIP	DIP	MP <sub>1</sub>	MP <sub>2</sub>	PIP	DIP	
Empty hand	0.01	0.08	0.53	0.31	0.31	0.02	1.65	1.23	0.05	0.56	0.36	-	2.73	1.46	0.56	-	1.62	1.06	0.86	
Ladybug	0.06	0.11	0.19	0.69	0.05	0.06	0.15	0.33	0.08	0.16	0.58	-	0.04	2.85	1.84	-	0.24	1.91	1.62	
Coke can	0.05	0.29	1.81	2.07	0.1	0.13	0.87	1.14	0.13	1.48	1.77	-	0.04	3.94	3.08	-	0.5	2.26	<b>4.24</b>	
Bottle	0.04	0.22	1.56	1.64	0.06	0.1	0.97	1.27	0.18	1.47	1.86	-	0.22	1.35	1.89	-	0.35	1.16	2.52	

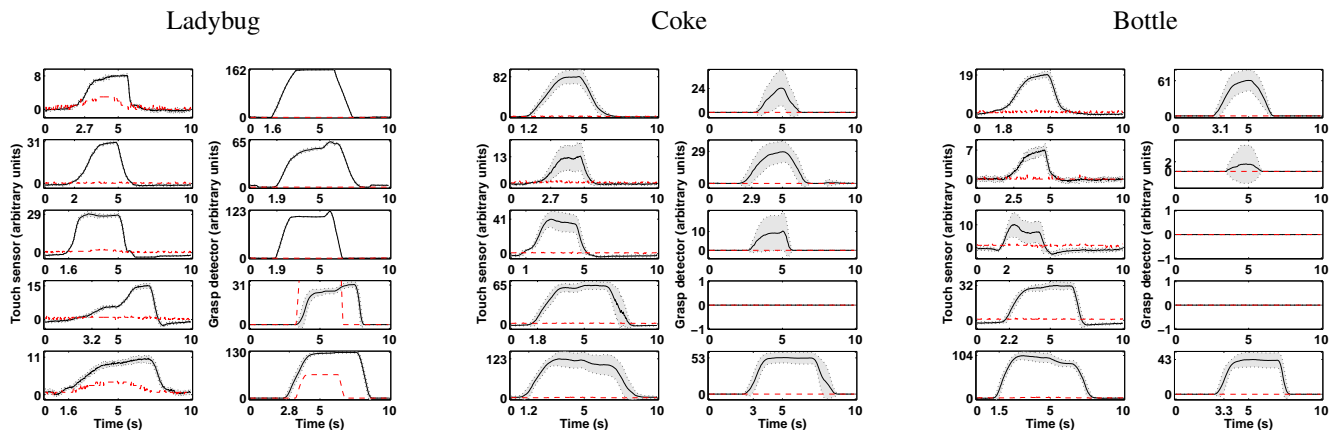


Fig. 10. A plot of the fingertips response (left columns) and grasp detector response (right columns) while grasping the three different objects in Fig. 1. Rows correspond to different fingers: from the top to the bottom, thumb, index, middle, ring and little. The red line is the response when the grasp action is performed with no object (when performing the ladybug grasping movement, thumb and little fingers mildly respond even if no object is present; these responses are due to imperfect grounding of the fingertip external conductive layer which produce a minor crosstalk disturbance). The black line is the average response in 20 trials. The shaded region is the standard deviation in 20 trials. The horizontal axis reports also the detection time instant; this instant has been obtained on the basis of a threshold chosen on a 95% confidence interval.

by motors embedded in the forearm and controlled by control boards housed in the upper arm. The final solution relies on 9 tendon actuated DOMs, custom electronic boards embedded in the hand and position/tactile sensors integrated in the fingertip/palm. Preliminary experiments have been conducted to quantify the reliability of the hand actuation and sensorization. Future works will focus on integrating tendon tension measurements so as to be able to quantify the force exerted by the fingertips on the object.

## VI. ACKNOWLEDGMENTS

This work was supported by the following EU projects: ITALK (FP7-ICT-2007.2.1), CHRIS (FP7-IST-215805) and ROBOSKIN (ICT-FP7-231500).

## REFERENCES

- [1] J. J. Gibson, *The Theory of Affordances*. Lawrence Erlbaum, 1977.
- [2] P. Cisek, "Beyond the computer metaphor: behavior as interaction," *Journal of Consciousness Studies*, vol. 6, no. 12, pp. 125–142, 1999.
- [3] G. Metta and P. Fitzpatrick, "Better vision through manipulation," *Adaptive Behavior*, vol. 11, no. 2, pp. 109–128, June 2003. [Online]. Available: <http://dx.doi.org/10.1177/10597123030112004>
- [4] S. Jacobsen, J. Wood, D. Knutti, and K. Biggers, "The UTAH/MIT dextrous hand: Work in progress," *The International Journal of Robotics Research*, vol. 3, no. 4, pp. 21–50, 1984.
- [5] C. S. Lovchik and M. A. Diftler, "Robonaut hand: a dextrous robot hand for space," in *Proc. IEEE Int. Conf. on Robotics and Automation (ICRA)*, vol. 2, 1999, pp. 907–912.
- [6] H. Liu, P. Meusel, N. Seitz, B. Willberg, G. Hirzinger, M. Jin, Y. Liu, R. Wei, and Z. Xie, "The modular multisensory DLR-HIT-hand," *Mechanism and Machine Theory*, vol. 42, no. 5, pp. 612–625, May 2007.
- [7] Shadow Hand Company. (2008) Shadow dexterous hand. [Online]. Available: [www.shadowrobot.com/hand/](http://www.shadowrobot.com/hand/)
- [8] L. Natale and E. Torres-Jara, "A sensitive approach to grasping," in *Proc. 6th Int. Conf. on Epigenetic Robotics*, 2006.
- [9] L. Biagiotti, F. Lotti, G. Palli, P. Tiezzi, G. Vassura, and C. Melchiorri, "Development of UB hand 3: Early results," in *Proc. IEEE Int. Conf. on Robotics and Automation (ICRA)*, 2005, barcelona, Spain, April 18.
- [10] N. Tsagarakis, G. Metta, G. Sandini, D. Vernon, R. Beira, J. Santos-Victor, M. Carrazzo, F. Becchi, and D. Caldwell, "iCub - the design and realization of an open humanoid platform for cognitive and neuroscience research," *International Journal of Advanced Robotics*, vol. 21, no. 10, pp. 1151–75, Oct. 2007.
- [11] G. Metta, G. Sandini, D. Vernon, L. Natale, and F. Nori, "The iCub humanoid robot: an open platform for research in embodied cognition," in *PerMIS: Performance Metrics for Intelligent Systems Workshop*, Washington DC, USA, Aug 19-21, 2008.
- [12] G. Stellan, G. Cappiello, S. Roccella, M. C. Carrozza, P. Dario, G. Metta, G. Sandini, , and F. Becchi, "Preliminary design of an anthropomorphic dexterous hand for a 2-years-old humanoid: towards cognition," in *Proc. IEEE BioRob*, 2006.
- [13] G. Stellan, C. Cipriani, F. Zaccone, M. Carrozza, and P. Dario, "Design of an anthropomorphic dexterous hand for a 2-years-old humanoid: Ongoing work," in *Proc. RoManSy*, 2008.
- [14] L.-W. Tsai, *Robot Analysis: The Mechanics of Serial and Parallel Manipulators*. Wiley-IEEE, 1999.
- [15] CarlStahl. stain-steel wires. [Online]. Available: <http://www.carlstahl.de>
- [16] Royal DSM. Dyneema synthetic fiber. [Online]. Available: <http://www.dyneema.com>
- [17] M. Santello, M. Flanders, and J. F. Soechting, "Postural hand synergies for tool use," *Journal of Neuroscience*, vol. 18, no. 23, pp. 10 105–10 115, December 1998.
- [18] iCub open source software repository documentation. [Online]. Available: <http://eris.liralab.it/iCub/dox/html/index.html>
- [19] A. Schmitz, M. Maggiali, L. Natale, and G. Metta, "Touch sensors for humanoid hands," in *Proc. 19th IEEE Int. Symposium in Robot and Human Interactive Communication (Ro-Man)*, 2010.